Cardiac Microlesions Form During Severe Bacteremic *Enterococcus faecalis* Infection

Armand O. Brown[1], Kavindra V. Singh[2], Melissa R. Cruz[1], Karan Gautam Kaval[1], Liezl E. Francisco[3], Barbara E. Murray[1,2], and Danielle A. Garsin[1*]

[1]Department of Microbiology and Molecular Genetics, The University of Texas Health Science Center at Houston, Houston TX, USA

[2] Division of Infectious Diseases, Department of Internal Medicine, The University of Texas Health Science Center at Houston, Houston, TX, USA

[3] Department of Biochemistry and Structural Biology, The University of Texas Health Science Center at San Antonio, San Antonio, TX, USA

*Corresponding author
Danielle.A.Garsin@uth.tmc.edu
713-500-5454

Running Title: Cardiac microlesions formed by *E. faecalis*

Abstract

Enterococcus faecalis is a significant cause of hospital-acquired bacteremia. Herein, the discovery is reported that cardiac microlesions form during severe bacteremic *E. faecalis* infection in mice. The cardiac microlesions were identical in appearance to those formed by *Streptococcus pneumoniae* during invasive pneumococcal disease (IPD). However, *E. faecalis* does not encode the virulence determinants implicated in pneumococcal microlesion formation. Rather, disulfide bond forming protein DsbA was found to be required for *E. faecalis* virulence in a *C. elegans* model and was necessary for efficient cardiac microlesion formation. Furthermore, *E. faecalis* promoted cardiomyocyte necroptotic cell death at sites of microlesion formation. Additionally, loss of DsbA caused an increase in pro-inflammatory cytokines unlike the wild type strain, which suppressed the immune response. In conclusion, we establish that *E. faecalis* is capable of forming cardiac microlesions and identify features of both the bacterium and the host response that are mechanistically involved.

KEYWORDS: Enterococcus faecalis, cardiac, microlesions, sepsis, bacteremia, infection, virulence, thioredoxin, disulfide bond, necroptosis

ABSTRACT WORD COUNT: 147

TEXT WORD COUNT: 3,478

64 **Introduction**

65

66 *Enterococcus faecalis* is a Gram-positive bacterium that normally co-exists with the host as a
67 harmless commensal. However, it is capable of causing a variety of infections such as infective
68 endocarditis (IE), urinary tract infection (UTI), bacteremia, peritonitis, prosthetic joint infection, and
69 endophthalmitis. A common complication associated with enterococcal bacteremia is
70 endocarditis, an infection that has a 1-year mortality rate of approximately 29% despite antibiotic
71 therapy [6]. Enterococci are the third most common cause of endocarditis in North America [8]
72 and, in patients with this infection, heart failure has been observed to occur with increased
73 frequency [9-15]. Infective endocarditis involves the formation of biofilms on heart valves and
74 inner chambers that develop into complex masses called vegetations [16]. Thus, heart infections
75 associated with *E. faecalis* have traditionally been characterized as occurring on the surfaces of
76 the heart, rather than in the deeper myocardial tissue, which would require active invasion.

77

78 Interestingly, another important Gram-positive pathogen, *Streptococcus pneumoniae,* was
79 recently shown to invade the heart tissue and form cardiac microlesions during invasive
80 pneumococcal disease (IPD) [17]. Importantly, pneumococcal microlesions were shown to be
81 associated with altered cardiac electrophysiology, heart failure and scar formation during
82 convalescence, which is thought to predispose individuals to major adverse cardiac events
83 (MACE) [17, 18]. Furthermore, cardiac microlesions form following vascular endothelial cell
84 invasion into the myocardial tissue through the interactions of pneumococcal Choline binding
85 protein A (CbpA) and pneumococcal teichoic acid associated phosphorylcholine (ChoP) with host
86 laminin receptor (LR) and platelet activating factor receptor (PAFr), respectively. Cardiomyocyte
87 death is mediated by exposure to the pneumococcal secreted cholesterol-dependent pore forming
88 toxin, pneumolysin [17, 18], and hydrogen peroxide [19, 20]. Since the original observation of

89 pneumococcal microlesions in 2014, similar observations were seen during blood stream
90 infections with *Francisella tularensis* [21], and *Mycobacterium avium* [22] , however the
91 mechanisms involved were not characterized.
92
93 In this report, we show that cardiac microlesions also form during invasive *E. faecalis* infection.
94 The observed cardiac microlesions were identical in appearance and size to *S. pneumoniae*
95 mediated cardiac microlesions, were diffuse across the myocardium, and characterized by an
96 absence of immune cell infiltration. Furthermore, an enterococcal determinant required for
97 microlesion formation, DsbA, was identified. Finally, *E. faecalis* infection of cardiomyocytes was
98 discovered to cause necroptosis and suppress the immune response.
99
100

Materials and Methods

C. elegans survival assay

E. faecalis strains were tested in *C. elegans* for survival as previously described [44]. The data is representative of 3 independent experiments. Nematode survival was plotted with the log-rank (Mantel-Cox) method using Prism 7 statistical software (GraphPad).

Bacterial strains and growth analysis

All *E. faecalis* strains used in this project were used in previously published studies [23] and are listed in Table S1. For growth analysis, overnight cultures were diluted to an OD_{600nm} of 0.05 in brain heart infusion (BHI) agar medium (Difco) in a volume of 200µl / well in a 96-well plate. The 96-well plate containing the diluted cultures were placed in a prewarmed 37ºC BioTek Cytation 5 plate reader, and OD_{600nm} measurements were taken every 10 minutes for 15 hours.

Mouse peritonitis and cardiac microlesion model

The mouse peritonitis model was performed as described previously [45]. The method for identifying and evaluating cardiac microlesion formation was conducted as described previously [17]. Briefly, female, ~4 – 6-week old (~25g), ICR outbred mice were obtained from Envigo (Indianapolis, Indiana) and infected intraperitoneally with $7x10^8$ CFUs of *E. faecalis*. Mouse hearts were obtained 24-48 hours post-infection, formalin fixed and sent to The University of Texas Health Science Center Histopathology Laboratory for paraffin embedding, sectioning, and hematoxylin and eosin H&E) staining. Paraffin embedded mouse hearts were first bisected and sectioned longitudinally. 20 sections were cut per block, and every 5th section H&E stained in order to measure the number and relative distribution of the microlesions. Cardiac microlesions were averaged across sections, and the differences between mouse groups compared using

126 *Student's* two-tailed t-test. Experiments were performed in accordance with protocols approved
127 by the Animal Welfare Committee of the University of Texas Health Science Center at Houston
128 AWC-19-0058.
129
130 **Necroptosis inhibition assay**
131 HL-1 cardiomyocytes were seeded in 24-well plates at a concentration of $5x10^5$ cells/ml. 24 hours
132 later, the cells were washed three times with Dulbecco's (1X) PBS, followed by pretreatment with
133 antibiotic free Claycomb medium supplemented with 10 μM of Necrostatin-1 (Sigma Aldrich),
134 GSK'872 (RD Systems), and Necrosulfonamaide (Millipore-Sigma) for 1 hour, followed by
135 infection at an MOI of 10 for 4 hours, following which the supernatant was collected, and
136 cytotoxicity in each well accessed using the CytoTox-ONE™ Homogeneous Membrane Integrity
137 Assay Kit (Promega). Each experiment was conducted in triplicate, on 3 separate occasions, and
138 averaged values between groups compared using *Student's* two-tailed t-test.
139
140 **Annexin V apoptosis and necrosis assay.**
141 The annexin V apoptosis and necrosis assay was conducted using RealTime-Glo™ Annexin V
142 Apoptosis and Necrosis Assay Kit (Promega). The kit contains near-equimolar ratios of two
143 annexin V fusion proteins (Annexin V-LgBiT and Annexin V-SmBit) containing complementary
144 subunits of NanoBiT® Luciferase that, when combined following exposure to phosphatidyl serine,
145 results in an emission of a luminescent signal. The kit also contains a cell-impermeant
146 profluorescent DNA dye, which detects necrosis. Briefly, HL-1 cardiomyocytes (Sigma-Aldrich)
147 were seeded in a 96 well plate. 24 hours later, the cells were infected with *E. faecalis* at an MOI
148 = 50, in the presence of kit reagents. Luminescent and fluorescent readings were obtained every
149 30 minutes for up to 6 hours.
150

151 **Invasion assay**

152 SVEC4-10 Endothelial Cells (ATCC) were seeded in 24 well plates at a cell density of $1.5x10^5$
153 cells/ml. After 24 hours, the cells were washed three times with PBS and infected with *E. faecalis*
154 at a MOI of 10 for 4 hours in antibiotic free Claycomb medium. After the incubation, the cells were
155 washed with Dulbecco's (1X) PBS three times and treated with trypsin, diluted in PBS, and plated
156 on BHI agar plates for attachment quantification. To measure intracellular numbers of *E. faecalis*,
157 cells that were washed three times with Dulbecco's (1X) PBS 4 h.p.i., then treated with Dulbecco's
158 Modified Eagle's Medium (ATCC) supplemented with 15 µg/ml vancomycin and 150 µg/ml
159 gentamicin. 24 hours later, the wells were washed three times with Dulbecco's (1X) PBS, lysed
160 using 0.1% Triton-X-100, and diluted and plated on BHI agar plates for intracellular quantification.
161 The ratio of invasion to attachment for a given enterococcal strain was used to calculate the
162 percent of invasion. The experiments were conducted on 3 independent occasions and were
163 performed using triplicate wells for each strain. Attachment and invasion values were averaged
164 from each experiment, and statistically analyzed using *Student's* two-tailed t-test.

165

166 **Cytotoxicity and inflammatory cytokine panel microtiter plate reader assay**

167 HL-1 cardiomyocytes were obtained from Sigma-Aldrich and SVEC4-10 Endothelial Cells were
168 obtained from ATCC. HL-1 cardiomyocytes (Sigma-Aldrich) were seeded into 24-well plates at a
169 concentration of $5x10^5$ cells/ml. 24 hours later, the cells were washed three times with Dulbecco's
170 (1X) PBS, and infected with *E. faecalis* at an MOI of 10 for 4 hours in antibiotic free Claycomb
171 medium. Supernatant was collected, and cytotoxicity assayed using CytoTox-ONE™
172 Homogeneous Membrane Integrity Assay Kit (Promega). In addition to measuring cytotoxicity in
173 HL-1 cardiomyocytes infected with *E. faecalis* 4 h.p.i, inflammatory chemokines and cytokines
174 were analyzed using a Mouse Cytokine ELISA Plate Array III Colorimetric Assay (Signosis). The

175 data represent an average of at least 3 independent experiments for each isogenic mutant tested
176 and were analyzed using *Student's* two-tailed t-test.
177
178 **Immunofluorescence microscopy**
179 Immunofluorescence microcopy was conducted as described previously [17]. Briefly, paraffin
180 embedded sections were treated with 1:100 rabbit Anti-mouse MLKL (phospho S345) antibody
181 [EPR9515(2)] in order to detect phosphorylated MLKL (Abcam), and 1:100 rat anti-mouse MLKL
182 antibody (Millipore-Sigma) for MLKL detection followed by treatment with 1:1000 chicken anti-
183 rabbit IgG (H+L) cross-adsorbed secondary Alexa Fluor 594 antibody (ThermoFisher), and 1:1000
184 goat anti-rat IgG (H+L) secondary FITC antibody (ThermoFisher) respectively. A rabbit anti-
185 *Enterococcus faecalis* antibody (Abcam) was used at a concentration of 1:1000 to detect *E.*
186 *faecalis* within cardiac microlesions followed by treatment with 1:1000 goat anti-rabbit IgG (H&L),
187 FITC conjugated antibody (Invitrogen). All stained sections were counterstained with 1:1000 DAPI
188 (ThermoFisher) and mounted with Hardset™ Antifade Mounting Medium. Visualization of
189 fluorescence was obtained using standard excitation and emission wavelengths for Alexa 594,
190 FITC, and DAPI on an Olympus FV3000RS high-speed, high-sensitivity, inverted laser scanning
191 confocal microscope.
192
193 **Generation of rabbit anti-DsbA antisera**
194 His-tagged recombinant DsbA was overexpressed in Rosetta-2(DE3) *E. coli* (Sigma-Aldrich) and
195 isolated by affinity purification via HisPur Nickel-NTA Resin (ThermoFisher) packed columns
196 followed by further purification and buffer exchange using Fast Protein Liquid Chromatography
197 (FPLC) to obtain highly pure samples of recombinant DsbA. Cocalico Biologicals (Reamstown,
198 PA) generated anti-DsbA antisera by immunizing rabbits with the recombinant protein.
199

200 ***E. faecalis* whole cell lysate and Western blot**

201 An overnight culture of *E. faecalis* grown in BHI medium was centrifuged, washed with BHI and
202 then diluted 1/100 in 5 ml of BHI. The culture was subsequently incubated at 37ºC for an additional
203 3.5 hours to obtain a culture of *E. faecalis* in exponential growth. The culture was spun down and
204 the supernatant removed. Following sonication of the pellet, the sample was centrifuged at 10,000
205 G for 5 minutes and supernatant collected for electrophoresis. Following electrophoresis and
206 transfer of protein to a PVDF membrane, the membrane was incubated overnight at 4ºC in a 5%
207 milk solution containing a 1:1000 dilution of rabbit anti-DsbA antisera followed by incubation with
208 a Goat anti-rabbit IgG HRP (ThermoFisher) secondary antibody at a dilution of 1:10,000 at room
209 temperature for 30 minutes prior to development with a chemiluminescent kit (ThermoFisher).
210

211 **Results**

212

213 **Cardiac microlesions form during severe bacteremic *E. faecalis* infection.** In previous work,
214 we implicated a previously uncharacterized *E. faecalis* thioredoxin known as DsbA (disulfide bond
215 forming protein A) as a requirement for the stability of EntV, a secreted bacteriocin that we
216 determined inhibits hyphal morphogenesis of the human fungal pathogen *Candida albicans* [23,
217 24]. To test if these proteins had any effects on the fitness and pathogenicity of *E. faecalis*, we
218 infected *Caenorhabditis elegans* with *ΔdsbA* and *ΔentV E. faecalis* mutants and measured
219 survival. As shown in Figure 1A, loss of *dsbA* significantly attenuated mortality in infected
220 nematodes. Note that the *ΔdsbA* mutant did not manifest different growth kinetics when grown in
221 culture medium compared to wild type, ruling out a general growth defect (Figure S1). Infection
222 with the complement, *ΔdsbA::dsbA*, partially rescued the *ΔdsbA* phenotype. The partial
223 complementation was attributed to the DsbA protein being produced at lower levels in the
224 complemented strain (Figure 1B). No significant difference in nematode survival was observed
225 following infection with either the *ΔentV* mutant or its complement (Fig. 1A). Considering that EntV
226 is the only known substrate of *E. faecalis* DsbA, the results suggest that DsbA has additional
227 targets that affect pathogenicity.

228

229 Based on these results, we wanted to know if loss of DsbA also affected virulence in a vertebrate
230 animal model of *E. faecalis* infection. Therefore, the mutants were tested in a mouse model in
231 which animals were injected intra-peritoneally with *E. faecalis* resulting in generalized bacteremia
232 leading to mortality. Significant survival differences between the mice infected with the different
233 strains were not observed. However, various organs were collected in order to determine if *E.*
234 *faecalis* infection induced any strain-specific, pathological effects. To our surprise, cardiac
235 microlesions were discovered within the myocardium that were devoid of immune cell infiltrate

236 (Fig. 2 A, B). The microlesions appeared to form within roughly the same time frame (~24 h.p.i.)
237 as cardiac microlesions that have previously been reported to occur during invasive infection with
238 *S. pneumoniae*, the only other pathogen known to cause cardiac microlesions to date [17].
239
240 To verify that the observed microlesions were the result of infection by *E. faecalis*,
241 immunofluorescent staining on paraffin embedded cardiac tissue sections from mice infected with
242 *E. faecalis* with a polyclonal anti-enterococcal IgG antibody was performed and revealed the
243 presence of dense aggregates of *E. faecalis* within the microlesions (Fig. 2C). The presence of
244 bacterial DNA was further verified by DNA counterstaining with DAPI that revealed an
245 accumulation of non-cardiomyocyte nuclear DNA within microlesions (Fig. 2D). To determine the
246 contribution of DsbA toward microlesion formation, cardiac microlesions found on hematoxylin
247 and eosin stained paraffin embedded cardiac sections were quantified following infection with
248 Δ*dsbA*. A significant attenuation in microlesion formation during infection with *ΔdsbA* was
249 observed relative to wild type, while no significant difference was observed in mice infected with
250 the *dsbA* complement (Fig. 2E). Furthermore, when the sizes of the cardiac microlesions were
251 compared, the wild-type lesions were significantly larger than those found in the Δ*dsbA* infected
252 mice (Fig. 2F). Importantly, the size of the microlesions appeared to correlate with level of *dsbA*
253 expression observed in Western blots of *E. faecalis* whole cell lysates (Fig. 1B), with the
254 *ΔdsbA::dsbA* strain manifesting an in-between phenotype to that of the *ΔdsbA* and wild-type
255 strains, consistent with partial complementation. In conclusion, these data demonstrate that
256 cardiac microlesion formation occurs during systematic infection with *E. faecalis* and is dependent
257 on DsbA.
258
259 **Necroptosis contributes to cardiomyocyte cell death within microlesions.** In previous
260 studies of pneumococcal cardiac microlesion formation, apoptosis was found to be associated

261 with microlesion formation in mice (22). A subsequent study determined that cardiomyocyte cell
262 death occurs following exposure to pneumolysin (*ply*) and pneumococcal derived hydrogen
263 peroxide (*spxB*) [20]. Based on these observations and the fact that *E. faecalis* lacks *ply* and *spxB*
264 homologs, we sought to determine whether *E. faecalis* could promote cell death of
265 cardiomyocytes and identify the mechanism. First, HL-1 cardiomyocytes were infected with *E.*
266 *faecalis* and subsequently lactate dehydrogenase (LDH) release into the cell culture supernatant
267 was measured to assess cell death. From these experiments, it was concluded that *E. faecalis*
268 induces cell death of cardiomyocytes. Furthermore, infection with a *ΔdsbA* mutant resulted in a
269 significant decrease in cardiomyocyte cell death (Fig. 3B), suggesting DsbA is required to
270 modulate this process. Since cardiomyocyte cell death was observed following exposure to *E.*
271 *faecalis*, we wanted to identify the mechanism. To test this question, an annexin V apoptosis and
272 necrosis assay was performed to determine if *E. faecalis* promotes apoptosis or necrosis during
273 cardiomyocyte infection. The signals for both apoptosis and necrosis increased concomitantly
274 with time (Figure S2), suggesting that cell death is occurring by an apoptosis-independent
275 mechanism (see Materials and Methods). One apoptosis-independent cell death pathway is
276 necroptosis, and this mechanism of cell death is consistent with data published by investigators
277 studying *S. pnuemoniae* microlesions, which showed that markers of necroptosis could be
278 detected within the myocardium of acutely ill mice [17] and non-human primates [18]. Importantly,
279 necroptosis is considered a key cell death pathway in cardiomyocytes during ischemia-
280 reperfusion injury and acute coronary syndrome [25-27]. To test the hypothesis that
281 cardiomyocytes undergo necroptosis following exposure to *E. faecalis*, we infected HL-1
282 cardiomyocytes with this bacterium in the presence of various inhibitors of necroptosis and
283 observed a significant suppression of cell death (Fig. 3C). Additionally, staining for markers of
284 necroptosis [28], such as mixed lineage kinase domain-like pseudokinase (MLKL) and
285 phosphorylated MLKL, on cardiac tissue sections obtained from infected mice showed

286 concentrated signals within the microlesions (Fig 3D). Despite the ability of *E. faecalis* to promote
287 death of the cardiomyocytes following exposure, antibiotic protection assays indicated that the
288 bacteria were unable to invade cardiomyocytes relative to endothelial cells (Fig. 3A). No difference
289 was observed in either the ability to promote necroptosis or cell invasion following exposure to
290 *ΔdsbA* relative to wild-type (Figure S3). Taken together, these results suggest that during
291 bacteremia, *E. faecalis* is able to translocate across the vascular endothelium in order to enter
292 the myocardial tissue. Once there, *E. faecalis* is unable to invade cardiomyocytes, but can form
293 microcolonies that promote necroptotic cell death.

294 **Cardiomyocyte inflammatory cytokine response is suppressed following exposure to *E.***
295 ***faecalis*.** Cardiac microlesions are characterized by bacteria filled vacuoles that are largely devoid
296 of immune cell infiltrate [17, 29]. Previous efforts to explain the lack of an immune response to
297 pneumococcal microlesions have yielded interesting insights. For example, *S. pneumoniae* within
298 microlesions are thought to subvert the host response through a biofilm-mediated mechanism
299 involving the pneumolysin mediated killing of resident macrophages, thus creating a more
300 permissive environment for pneumococcal growth and survival [19]. There are also examples of
301 *E. faecalis* subverting the immune response. In previous work, it was shown that *E. faecalis* can
302 survive within mouse peritoneal macrophages for extended periods of time enabling the bacteria
303 to replicate and spread [30]. In more recent work, *E. faecalis* was shown to activate
304 Phosphatidylinositol 3-Kinase signaling that inhibits apoptosis [31]. *E. faecalis* can also resist
305 phagosome acidification and autophagy within macrophages [32]. Because *E. faecalis* does not
306 encode a pneumolysin homolog, nor does it secrete toxins known to kill macrophages or other
307 immune cells, we wanted to examine the immune response to *E. faecalis* within the heart by
308 measuring various inflammatory cytokines and chemokines. Experiments assessing
309 cardiomyocyte inflammatory chemokine and cytokine levels showed that wild-type *E. faecalis*
310 promotes an immune quiescent response, while loss of *dsbA* leads to a more inflammatory

311 immune response (Fig. 4A). Interestingly, EGF, M1P-1a, GM-CSF, IL-6, G-CSF, and INFr were
312 significantly upregulated during infection with *Δ*dsbA relative to the wild-type infected
313 cardiomyocytes. Thus, these results implicate the contribution of specific host signaling pathways
314 involved in pathogen clearance that are normally suppressed in the presence of DsbA during
315 infection, as modeled in Figure 4B. Collectively, these data suggest that *E. faecalis* inhibits a
316 vigorous cardiomyocyte immune response in a manner similar to that of *S. pneumoniae* despite
317 lacking the components that *S. pneumoniae* uses during immune subversion. Future studies will
318 be focused on understanding the cardiomyocyte immune response during enterococcal infection,
319 and how DsbA contributes.

320

321 **Discussion**

322

323 In this work, we demonstrated for the first time that cardiac microlesions form during severe *E.*
324 *faecalis* bacteremic infection of mice. Importantly, microlesions occurred despite *E. faecalis* not
325 encoding homologs of the pneumococcal virulence determinants implicated in microlesion
326 formation. These data suggest that *E. faecalis* may be expressing functionally redundant proteins
327 that serve to promote similar interactions to *S. pneumoniae* in mediating microlesion formation,
328 such as CbpA and pneumolysin, which facilitate vascular endothelial cell translocation and
329 cardiomyocyte cell death, respectively. Indeed, while *E. faecalis* does not encode a CbpA
330 homolog, it does encode other proteins capable of binding host extracellular matrix proteins.
331 These include EfbA, which binds fibronectin [33], ACE, which binds laminin receptor [34], and Ebp
332 pili that bind fibrinogen [35].

333

334 Interestingly, we did discover one factor, DsbA, that contributes to microlesion formation and
335 inhibition of the cardiomyocyte inflammatory immune response, as modeled in Figure 4B. Dsb
336 proteins work to catalyze disulfide bond formation in proteins and have been best studied in Gram-
337 negative bacteria where they catalyze the oxidative folding of proteins in the periplasm [36, 37].
338 While Dsb proteins and oxidative protein folding have established importance in the biology of
339 certain Gram-positive bacteria, like the Actinomyces, Dsb proteins are not well studied in
340 Firmicutes like *E. faecalis* and have generally not been considered important [36]. Most of these
341 species secrete few proteins containing cysteines and some, notably *S. pneumoniae*, do not
342 encode any thiol-disulfide oxidoreductases [38, 39]. A deletion of the only DsbA-like protein in *S.*
343 *aureus* resulted in no significant phenotypes including no effects on pathogenicity [40]. Thus, it
344 will be of interest to further investigate the role of Dsb proteins in these species.

345

346 Our prior work established EntV as a DsbA substrate, currently the only one identified [23].
347 However, loss of EntV did not reduce pathogenicity in the worm model (Figure 1A), and exposure
348 to EntV, even at very high concentrations, was non-toxic to mammalian cells [24]. Thus, we do
349 not favor EntV as being the source of DsbA's effects. A primary future direction will be to identify
350 additional substrates of DsbA and to determining which contribute to microlesion formation.
351
352 Pneumococcal ChoP interactions with host PAFr were determined to be a prerequisite for
353 vascular endothelial cell invasion during IPD. In light of our observations of *E. faecalis* invasion of
354 vascular endothelial cells despite an absence of this wall teichoic acid structure, it is possible that
355 another host receptor is required for endothelial cell invasion. Interestingly, recent studies focused
356 on bacterial cell wall entry and signaling in eukaryotic cells have identified a PAFr-independent
357 mechanism of tissue invasion that is actin-dependent and engenders Rac1, Cdc42, and
358 phosphatidylinositol 3-kinase (PI3K) signaling leading to cell wall internalization via a
359 macropinoctytosis-like pathway [41]. Whether such a pathway contributes to microlesion
360 formation is unknown. In the future, it will be of interest to study the mechanisms of tissue invasion
361 and the host signaling pathways involved.
362
363 Cardiac microlesion formation is becoming increasingly appreciated as a risk factor during acute
364 infection [42], and this study establishes that *E. faecalis* is another etiological agent capable of
365 causing this pathology in a vertebrate animal model. Considering that nosocomial derived
366 enterococcal infections are increasingly problematic among the elderly and immunocompromised
367 patients [4-7, 43], the development of successful treatments will require identifying all disease
368 manifestations as well as the bacterial and the host factors involved.
369
370
371

Table S1. Strains used in this study

***Enterococcus faecalis* Strains**				
Strain	**Genotype**	**Characteristics**	**Parent**	**Source**
OG1RF	Wild-type	Gel^+ Spr^+ Rf^R Fa^R	OG1	[46]
AOBD1	*ΔdsbA*	Gel^+ Spr^+ Rf^R Fa^R	OG1	[23]
AOBD2	*ΔdsbA::dsbA*	Gel^+ Spr^+ Rf^R Fa^R	OG1	[23]

421 **Figure Legends**

422

423 **Figure 1. *dsbA* deficient *E. faecalis* show reduced virulence in a *C. elegans* survival assay**.
424 **(A)** L4 stage *C. elegans* were infected with *E. faecalis*. This figure is representative of 3
425 independent experiments with 30 worms/group. ****Asterisk indicate a $P < 0.0001$ and were
426 analyzed by the log-rank (Mantel-Cox). **(B)** Western blot performed by SDS-PAGE separation of
427 *E. faecalis* whole cell lysates followed by hybridization of DsbA using rabbit anti-DsbA antisera.
428 Image is representative of 3 independent Western blot experiments.

429

430

431 **Figure 2. Cardiac microlesions form during invasive *E. faecalis* infection and are**
432 **attenuated by loss of *dsbA***. Cardiac microlesions were observed using light microscopy of
433 hematoxylin and eosin (H&E) stained paraffin embedded cardiac sections at 40X magnification
434 **(A)**, and 100X magnification **(B)**. Immunofluorescent detection of *E. faecalis* was imaged using a
435 20X objective at 3X zoom (total of 60X magnification), a FITC conjugated anti-enterococcal
436 antibody **(C)**, and DAPI for DNA staining **(D)**. Total microlesion counts **(E)**, and size measurements
437 **(F)**, were obtained by quantification using light microscopy of H&E stained paraffin embedded
438 cardiac sections from mice infected for 24-48 hours with *E. faecalis* (OG1RF n=14, Δ*dsbA* n=14,
439 Δ*dsbA::dsbA* n=14). The data were averaged from 3 independent experiments, and analyzed
440 using *Student's* two-tailed t-test (*** indicate a $P < 0.0001$).

441

442

443 **Figure 3. Necroptosis contributes to cardiotoxicity within cardiac microlesions**. **(A)**
444 Comparison of OG1RF invasion rates into HL-1 cardiomyocytes and SVEC endothelial cells. The
445 graph represents data from 3 independent experiments that were analyzed using *Student's* two-

446 tailed t-test (** indicate a $P < 0.01$). **(B)** *E. faecalis* induced cell death in HL-1 cardiomyocytes 4
447 hours post-infection (h.p.i.) as determined by measuring lactate dehydrogenase. The data
448 represent an average of 3 independent experiments and were analyzed using *Student's* two-tailed
449 t-test (* indicate a $P < 0.05$). **(C)** *E. faecalis* induced cell death in HL-1 cardiomyocytes 4 h.p.i. and
450 was inhibited in the presence of inhibitors of necroptosis. The data represent an average of 3
451 independent experiments and were analyzed using *Student's* two-tailed t-test (**** indicate a $P <$
452 0.0001). **(D)** Immunofluorescent microscopy of paraffin embedded cardiac cross sections at 20X
453 were performed to detect MLKL using FITC conjugated anti-MLKL antibodies, and Alexa 594
454 conjugated anti-phosphorylated MLKL antibodies at sites of microlesion formation, while DAPI
455 was used to stain nuclei.
456
457
458 **Figure 4. Wild-type *E. faecalis* suppresses the cardiomyocyte inflammatory response *in-***
459 ***vitro*. (A)** HL-1 cardiomyocytes exposed to *E. faecalis* promote a suppressed inflammatory
460 response while Δ*dsbA* infected cardiomyocytes yield a more inflammatory response. Data was
461 obtained from the fold-expression change analysis (relative to uninfected controls) of at least 3
462 independent experiments for each strain. **(B)** Model of *E. faecalis* mediated suppression of the
463 host cardiomyocyte immune response and effect on microlesion size.
464
465
466 **Supplemental Figure 1. *E. faecalis* growth curve.** *E. faecalis* strains were grown for 15 hours
467 in BHI and absorbance (OD_{600nm}) measured every 10 minutes. This figure is representative of 3
468 independent experiments.
469
470

471 **Supplemental Figure 2. Cardiomyocytes infected with *E. faecalis* die through an apoptosis**
472 **independent mechanism.** HL-1 cardiomyocytes were infected with *E. faecalis* at an MOI=50 for
473 4 hours in the presence of annexin V fusion proteins containing complimentary subunits of
474 NanoBiT® Luciferase combined with a cell-impermeant profluorescent DNA dye to detect
475 necrosis. A concomitant increase in both luminescent (apoptosis) **(A)** and fluorescent (necrosis)
476 **(B)** signals are indicative of cell death through an apoptosis independent mechanism. The graphs
477 represent an average of 3 independent experiments.
478
479
480 **Supplemental Figure 3. Loss of *dsbA* does has no effect on endothelial cell invasion or**
481 **necroptosis induced cell death of cardiomyocytes. (A)** Comparison of WT and *ΔdsbA* invasion
482 rates into HL-1 cardiomyocytes and SVEC endothelial cells showed no significant difference. The
483 graph represents data from 3 independent experiments analyzed using *Student's* two-tailed t-test
484 (NS denotes no significance). **(B)** Comparison of WT and *ΔdsbA* in HL-1 cardiomyocytes 4 h.p.i.
485 in the presence of inhibitors of necroptosis *in-vitro* was determined by measuring lactate
486 dehydrogenase. No significant difference was observed between necroptosis inhibitor conditions
487 tested. The data represent an average of 3 independent experiments and were analyzed using
488 *Student's* two-tailed t-test (* indicate a $P < 0.05$).
489
490
491
492
493
494
495
496
497

498 **References**

499

500 1. Lebreton F, Willems RJL, Gilmore MS. Enterococcus Diversity, Origins in Nature, and Gut
501 Colonization. In: Gilmore MS, Clewell DB, Ike Y, Shankar N, eds. Enterococci: From Commensals
502 to Leading Causes of Drug Resistant Infection. Boston, **2014**.
503 2. Armstrong-Evans M, Litt M, McArthur MA, et al. Control of transmission of vancomycin-resistant
504 Enterococcus faecium in a long-term-care facility. Infect Control Hosp Epidemiol **1999**; 20:312-7.
505 3. Goh HMS, Yong MHA, Chong KKL, Kline KA. Model systems for the study of Enterococcal
506 colonization and infection. Virulence **2017**; 8:1525-62.
507 4. Malani PN KC, Zervis MJ. Enterococcal disease, epidemiology and treatment. Washington,
508 D.C.: ASM Press, **2002** The Enterococci: Pathogenesis, Molecular Biology and Antibiotic
509 Resistance).
510 5. Wisplinghoff H, Bischoff T, Tallent SM, Seifert H, Wenzel RP, Edmond MB. Nosocomial
511 bloodstream infections in US hospitals: analysis of 24,179 cases from a prospective nationwide
512 surveillance study. Clin Infect Dis **2004**; 39:309-17.
513 6. Chirouze C, Athan E, Alla F, et al. Enterococcal endocarditis in the beginning of the 21st
514 century: analysis from the International Collaboration on Endocarditis-Prospective Cohort Study.
515 Clin Microbiol Infect **2013**; 19:1140-7.
516 7. McDonald JR, Olaison L, Anderson DJ, et al. Enterococcal endocarditis: 107 cases from the
517 international collaboration on endocarditis merged database. Am J Med **2005**; 118:759-66.
518 8. Agudelo Higuita NI, Huycke MM. Enterococcal Disease, Epidemiology, and Implications for
519 Treatment. In: Gilmore MS, Clewell DB, Ike Y, Shankar N, eds. Enterococci: From Commensals
520 to Leading Causes of Drug Resistant Infection. Boston, **2014**.
521 9. Cabell CH, Jollis JG, Peterson GE, et al. Changing patient characteristics and the effect on
522 mortality in endocarditis. Arch Intern Med **2002**; 162:90-4.

523 10. Garvey GJ, Neu HC. Infective endocarditis--an evolving disease. A review of endocarditis at
524 the Columbia-Presbyterian Medical Center, 1968-1973. Medicine (Baltimore) **1978**; 57:105-27.
525 11. Geraci JE, Martin WJ. Antibiotic therapy of bacterial endocarditis. VI. Subacute enterococcal
526 endocarditis; clinical, pathologic and therapeutic consideration of 33 cases. Circulation **1954**;
527 10:173-94.
528 12. Jawetz E, Sonne M. Penicillin-streptomycin treatment of enterococcal endocarditis. A re-
529 evaluation. N Engl J Med **1966**; 274:710-5.
530 13. Lerner PI, Weinstein L. Infective endocarditis in the antibiotic era. N Engl J Med **1966**;
531 274:388-93 concl.
532 14. Olaison L, Schadewitz K, Swedish Society of Infectious Diseases Quality Assurance Study
533 Group for E. Enterococcal endocarditis in Sweden, 1995-1999: can shorter therapy with
534 aminoglycosides be used? Clin Infect Dis **2002**; 34:159-66.
535 15. Pelletier LL, Jr., Petersdorf RG. Infective endocarditis: a review of 125 cases from the
536 University of Washington Hospitals, 1963-72. Medicine (Baltimore) **1977**; 56:287-313.
537 16. Garsin DA, Frank KL, Silanpaa J, et al. Pathogenesis and Models of Enterococcal Infection.
538 In: Gilmore MS, Clewell DB, Ike Y, Shankar N, eds. Enterococci: From Commensals to Leading
539 Causes of Drug Resistant Infection. Boston, **2014**.
540 17. Brown AO, Mann B, Gao G, et al. Streptococcus pneumoniae translocates into the
541 myocardium and forms unique microlesions that disrupt cardiac function. PLoS Pathog **2014**;
542 10:e1004383.
543 18. Reyes LF, Restrepo MI, Hinojosa CA, et al. Severe Pneumococcal Pneumonia Causes Acute
544 Cardiac Toxicity and Subsequent Cardiac Remodeling. Am J Respir Crit Care Med **2017**;
545 196:609-20.

546 19. Shenoy AT, Brissac T, Gilley RP, et al. Streptococcus pneumoniae in the heart subvert the
547 host response through biofilm-mediated resident macrophage killing. PLoS Pathog **2017**;
548 13:e1006582.
549 20. Brissac T, Shenoy AT, Patterson LA, Orihuela CJ. Cell Invasion and Pyruvate Oxidase-
550 Derived H2O2 Are Critical for Streptococcus pneumoniae-Mediated Cardiomyocyte Killing. Infect
551 Immun **2018**; 86.
552 21. Makara MA, Hoang KV, Ganesan LP, et al. Cardiac Electrical and Structural Changes During
553 Bacterial Infection: An Instructive Model to Study Cardiac Dysfunction in Sepsis. J Am Heart
554 Assoc **2016**; 5.
555 22. Headley CA, Gerberick A, Mehta S, et al. Nontuberculous mycobacterium M. avium infection
556 predisposes aged mice to cardiac abnormalities and inflammation. Aging Cell **2019**; 18:e12926.
557 23. Armand O. Brown CEG, Melissa R. Cruz, Michael C. Lorenz, Danielle A. Garsin. Antifungal
558 activity of the Enterococcus faecalis peptide EntV requires protease cleavage and disulfide bond
559 formation. Mbio **2019**; 10:1-13.
560 24. Graham CE, Cruz MR, Garsin DA, Lorenz MC. Enterococcus faecalis bacteriocin EntV inhibits
561 hyphal morphogenesis, biofilm formation, and virulence of Candida albicans. Proc Natl Acad Sci
562 U S A **2017**; 114:4507-12.
563 25. Zhang T, Zhang Y, Cui M, et al. CaMKII is a RIP3 substrate mediating ischemia- and oxidative
564 stress-induced myocardial necroptosis. Nat Med **2016**; 22:175-82.
565 26. Linkermann A, Hackl MJ, Kunzendorf U, Walczak H, Krautwald S, Jevnikar AM. Necroptosis
566 in immunity and ischemia-reperfusion injury. Am J Transplant **2013**; 13:2797-804.
567 27. Linkermann A, Brasen JH, Darding M, et al. Two independent pathways of regulated necrosis
568 mediate ischemia-reperfusion injury. Proc Natl Acad Sci U S A **2013**; 110:12024-9.
569 28. Kitur K, Wachtel S, Brown A, et al. Necroptosis Promotes Staphylococcus aureus Clearance
570 by Inhibiting Excessive Inflammatory Signaling. Cell Rep **2016**; 16:2219-30.

571 29. Gilley RP, Gonzalez-Juarbe N, Shenoy AT, et al. Infiltrated Macrophages Die of Pneumolysin-
572 Mediated Necroptosis following Pneumococcal Myocardial Invasion. Infect Immun **2016**; 84:1457-
573 69.
574 30. Gentry-Weeks CR, Karkhoff-Schweizer R, Pikis A, Estay M, Keith JM. Survival of
575 Enterococcus faecalis in mouse peritoneal macrophages. Infect Immun **1999**; 67:2160-5.
576 31. Zou J, Shankar N. Enterococcus faecalis infection activates phosphatidylinositol 3-kinase
577 signaling to block apoptotic cell death in macrophages. Infect Immun **2014**; 82:5132-42.
578 32. Zou J, Shankar N. The opportunistic pathogen Enterococcus faecalis resists phagosome
579 acidification and autophagy to promote intracellular survival in macrophages. Cell Microbiol **2016**;
580 18:831-43.
581 33. Singh KV, La Rosa SL, Somarajan SR, Roh JH, Murray BE. The fibronectin-binding protein
582 EfbA contributes to pathogenesis and protects against infective endocarditis caused by
583 Enterococcus faecalis. Infect Immun **2015**; 83:4487-94.
584 34. Nallapareddy SR, Qin X, Weinstock GM, Hook M, Murray BE. Enterococcus faecalis adhesin,
585 ace, mediates attachment to extracellular matrix proteins collagen type IV and laminin as well as
586 collagen type I. Infect Immun **2000**; 68:5218-24.
587 35. .Nallapareddy SR, Singh KV, Sillanpaa J, et al. Endocarditis and biofilm-associated pili of
588 Enterococcus faecalis. J Clin Invest **2006**; 116:2799-807.
589 36. Reardon-Robinson ME, Ton-That H. Disulfide-Bond-Forming Pathways in Gram-Positive
590 Bacteria. J Bacteriol **2015**; 198:746-54.
591 37. Landeta C, Boyd D, Beckwith J. Disulfide bond formation in prokaryotes. Nat Microbiol **2018**;
592 3:270-80.
593 38. Daniels R, Mellroth P, Bernsel A, et al. Disulfide bond formation and cysteine exclusion in
594 gram-positive bacteria. J Biol Chem **2010**; 285:3300-9.

595 39. Dutton RJ, Boyd D, Berkmen M, Beckwith J. Bacterial species exhibit diversity in their
596 mechanisms and capacity for protein disulfide bond formation. Proc Natl Acad Sci U S A **2008**;
597 105:11933-8.
598 40. Dumoulin A, Grauschopf U, Bischoff M, Thony-Meyer L, Berger-Bachi B. Staphylococcus
599 aureus DsbA is a membrane-bound lipoprotein with thiol-disulfide oxidoreductase activity. Arch
600 Microbiol **2005**; 184:117-28.
601 41. Loh LN, Gao G, Tuomanen EI. Dissecting Bacterial Cell Wall Entry and Signaling in Eukaryotic
602 Cells: an Actin-Dependent Pathway Parallels Platelet-Activating Factor Receptor-Mediated
603 Endocytosis. MBio **2017**; 8.
604 42. Musher DM, Abers MS, Corrales-Medina VF. Acute Infection and Myocardial Infarction. N
605 Engl J Med **2019**; 380:171-6.
606 43. Weiner LM, Webb AK, Limbago B, et al. Antimicrobial-Resistant Pathogens Associated With
607 Healthcare-Associated Infections: Summary of Data Reported to the National Healthcare Safety
608 Network at the Centers for Disease Control and Prevention, 2011-2014. Infect Control Hosp
609 Epidemiol **2016**; 37:1288-301.
610 44. Garsin DA, Sifri CD, Mylonakis E, et al. A simple model host for identifying Gram-positive
611 virulence factors. Proc Natl Acad Sci U S A **2001**; 98:10892-7.
612 45. Singh KV, Qin X, Weinstock GM, Murray BE. Generation and testing of mutants of
613 Enterococcus faecalis in a mouse peritonitis model. J Infect Dis **1998**; 178:1416-20.
614 46. Murray BE, Singh KV, Ross RP, Heath JD, Dunny GM, Weinstock GM. Generation of
615 restriction map of Enterococcus faecalis OG1 and investigation of growth requirements and
616 regions encoding biosynthetic function. J Bacteriol **1993**; 175:5216-23.
617
618
619

620 **FOOTNOTE PAGE**

621 **Conflict of Interest statement**

622 There are no conflicts of interest.

623 **Funding statement**

624 This work was supported by the National Institute of Dental and Craniofacial Research of the
625 National Institutes of Health under [grant number R01DE027608 to D. A. G.] and [grant number
626 F32DE027580 to A. O. B.]

627 **Meetings**

628 This work has not been presented.

629 **Corresponding author contact information**

630 Danielle A. Garsin, Ph.D.

631 6431 Fannin St.

632 MSB 1.168

633 Houston, TX 77030

634 Telephone: (713) 500-5454

635 Fax: (713) 500-5499

636 Email: Danielle.A.Garsin@uth.tmc.edu

637

A.

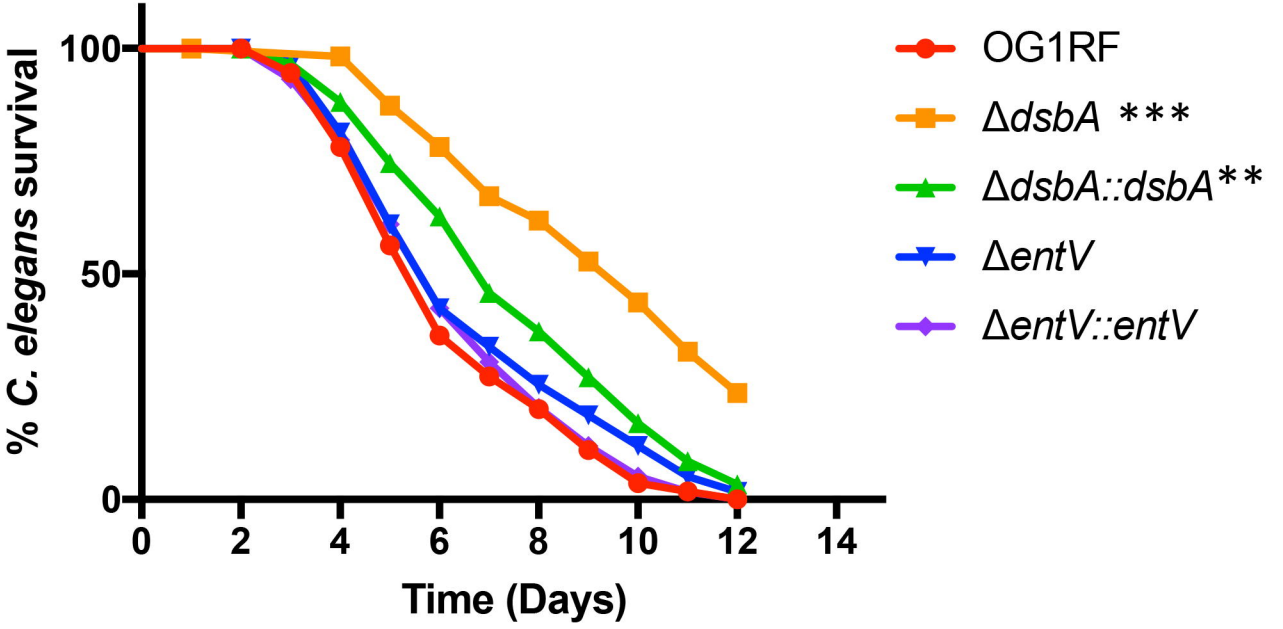
% C. elegans survival
100
50
0
0
2
4
6
8
10
12
14
Time (Days)
OG1RF
ΔdsbA ***
ΔdsbA::dsbA**
ΔentV
ΔentV::entV

B.

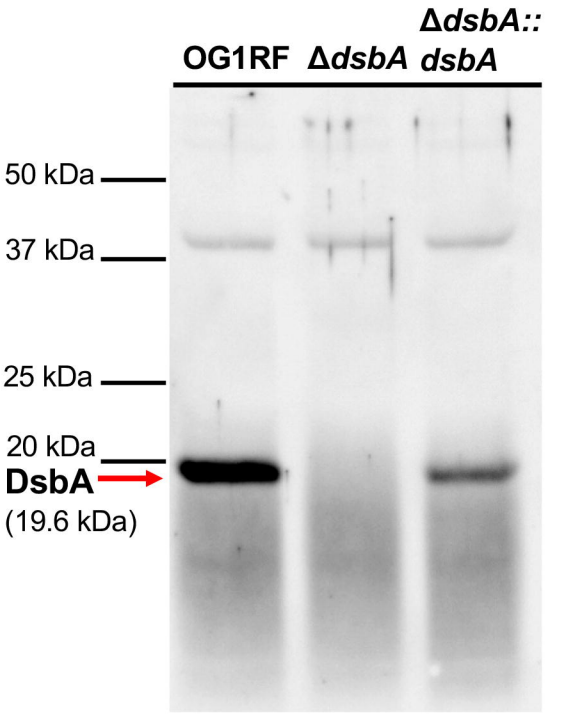
OG1RF
ΔdsbA
ΔdsbA::
dsbA
50 kDa
37 kDa
25 kDa
20 kDa
DsbA
(19.6 kDa)

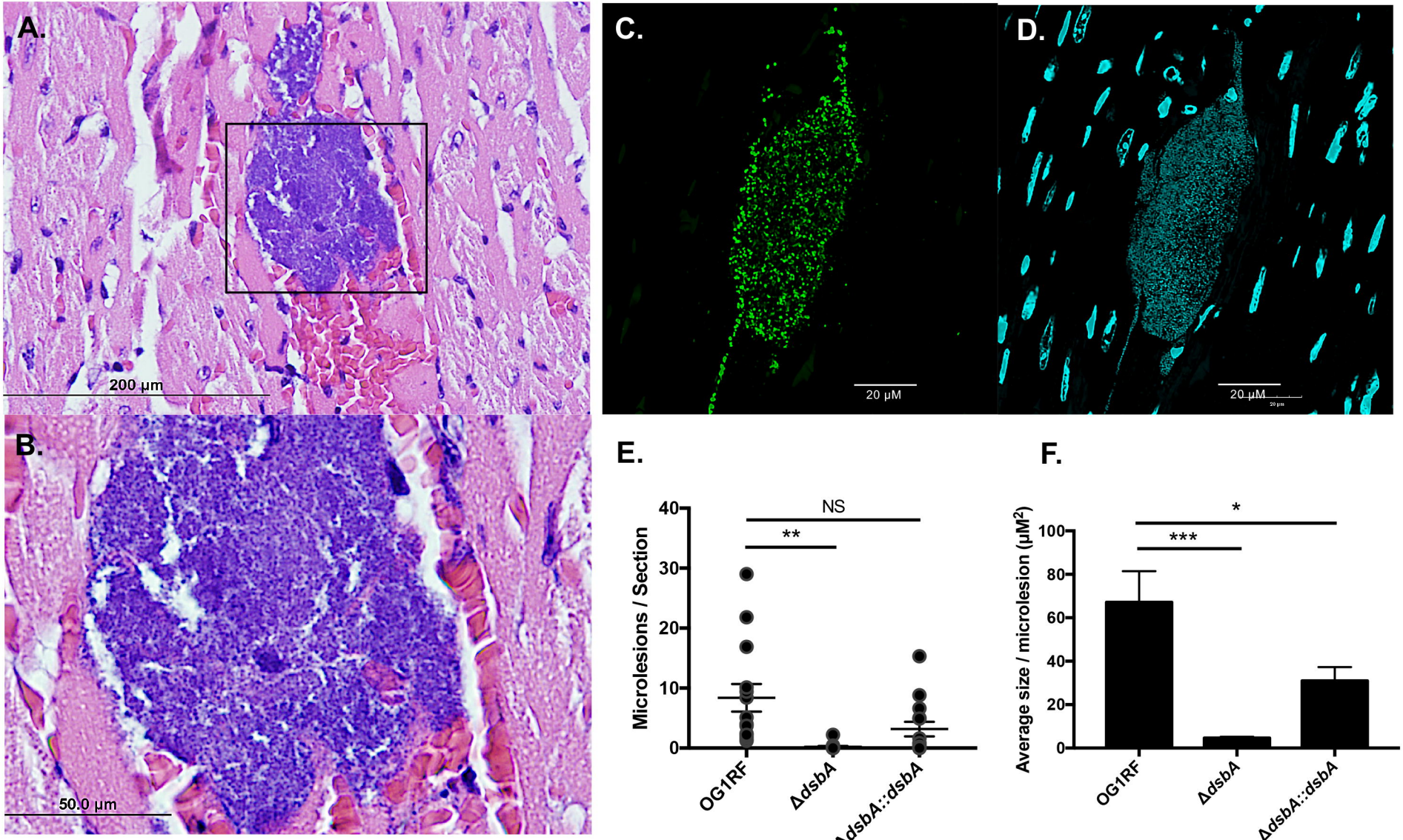
A.
200 µm
B.
50.0 µm
C.
20 µM
D.
20 µM
E.
Microlesions / Section
40
30
20
10
0
NS
**
OG1RF
ΔdsbA
ΔdsbA::dsbA
F.
Average size / microlesion (µM²)
100
80
60
40
20
0
*
***
OG1RF
ΔdsbA
ΔdsbA::dsbA

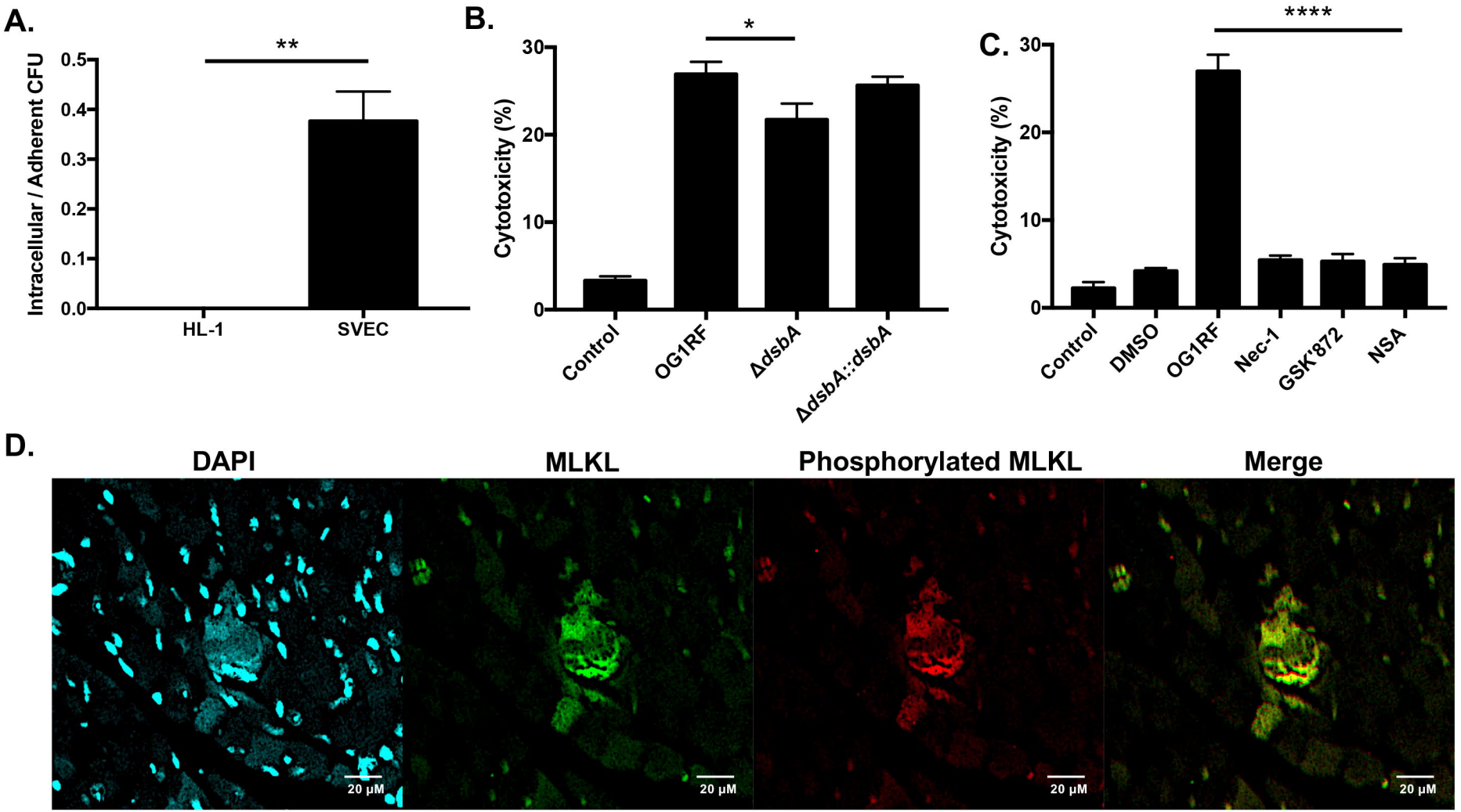
A.
**
Intracellular / Adherent CFU
0.5
0.4
0.3
0.2
0.1
0.0
HL-1
SVEC
B.
*
Cytotoxicity (%)
30
20
10
0
Control
OG1RF
ΔdsbA
ΔdsbA::dsbA
C.
****
Cytotoxicity (%)
30
20
10
0
Control
DMSO
OG1RF
Nec-1
GSK'872
NSA
D.
DAPI
MLKL
Phosphorylated MLKL
Merge
20 μM
20 μM
20 μM
20 μM

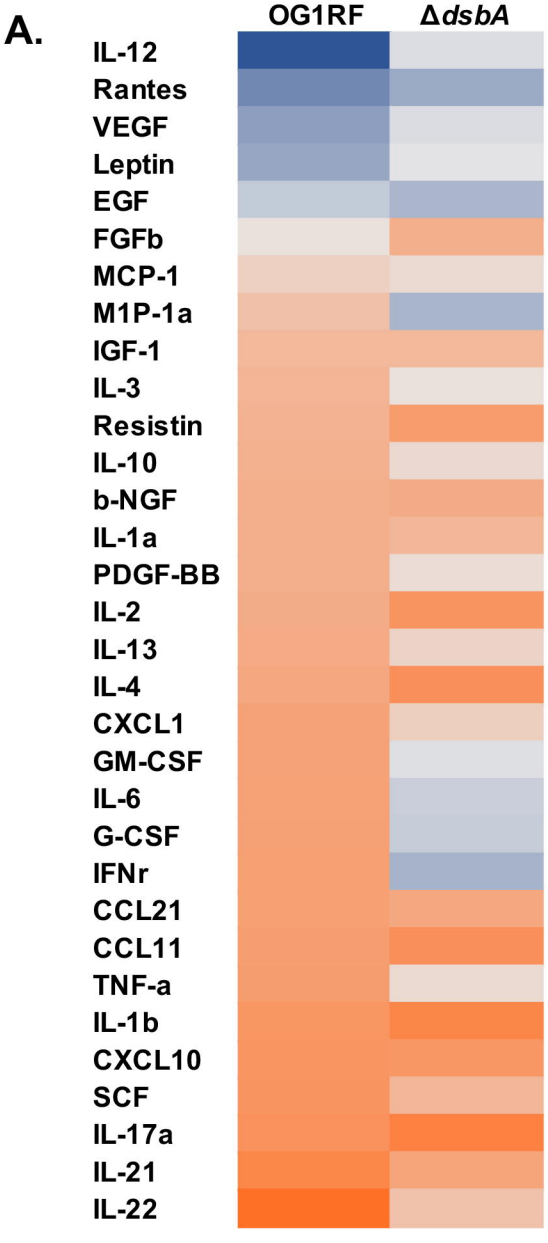
A.
OG1RF
ΔdsbA
IL-12
Rantes
VEGF
Leptin
EGF
FGFb
MCP-1
M1P-1a
IGF-1
IL-3
Resistin
IL-10
b-NGF
IL-1a
PDGF-BB
IL-2
IL-13
IL-4
CXCL1
GM-CSF
IL-6
G-CSF
IFNr
CCL21
CCL11
TNF-a
IL-1b
CXCL10
SCF
IL-17a
IL-21
IL-22

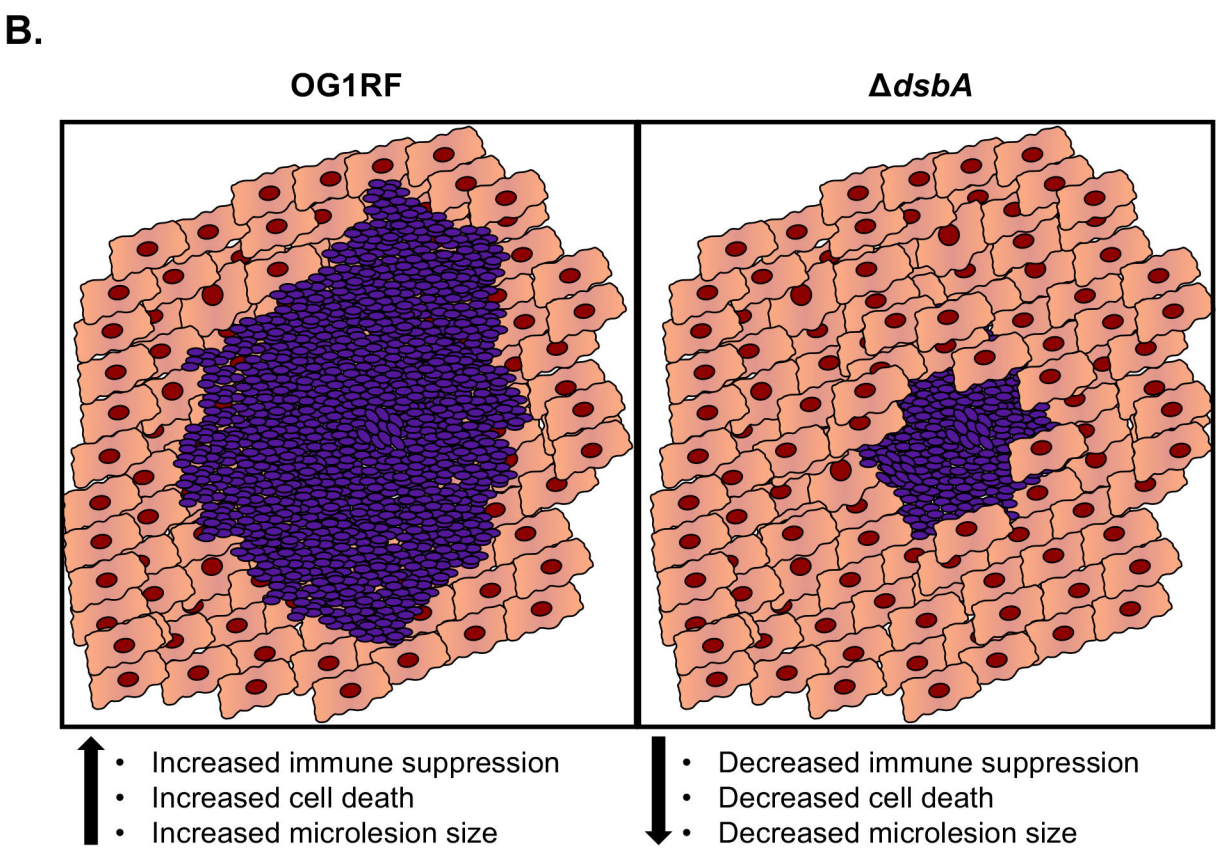
B.
OG1RF
ΔdsbA
• Increased immune suppression
• Increased cell death
• Increased microlesion size
• Decreased immune suppression
• Decreased cell death
• Decreased microlesion size

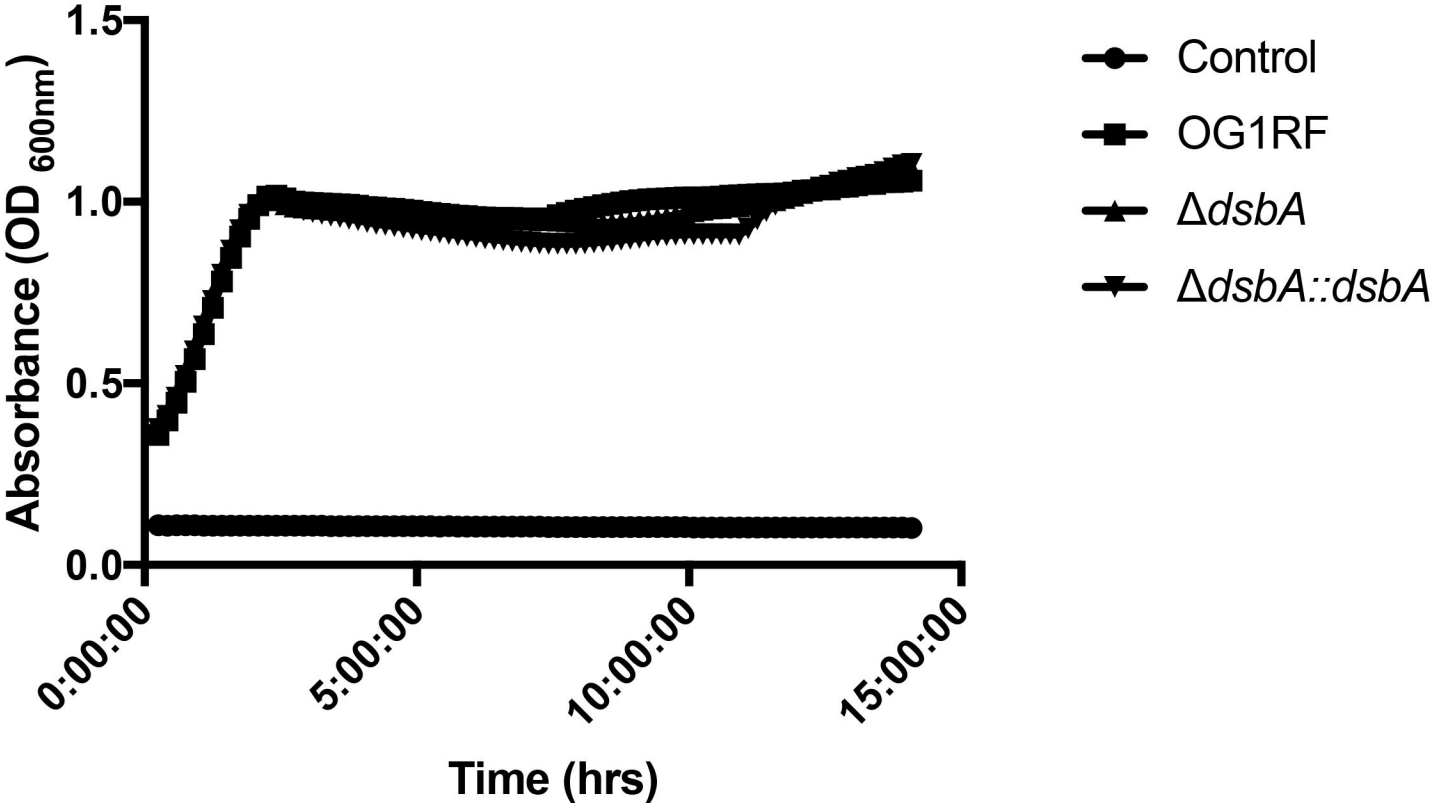
1.5
1.0
0.5
0.0
Absorbance (OD 600nm)
0:00:00
5:00:00
10:00:00
15:00:00
Time (hrs)
Control
OG1RF
ΔdsbA
ΔdsbA::dsbA

A.

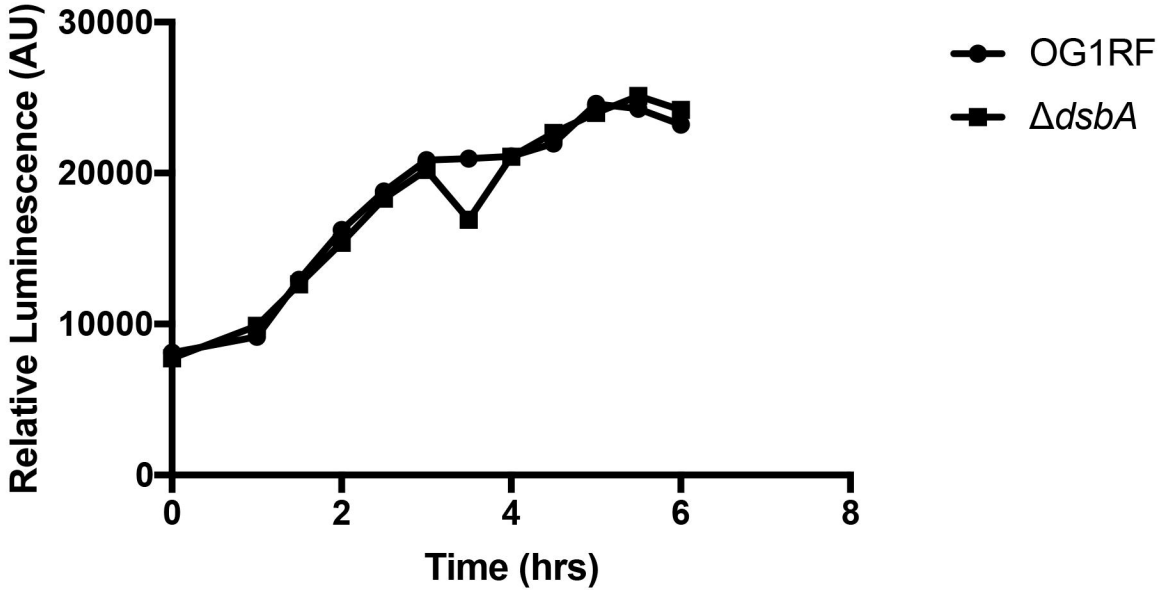
Relative Luminescence (AU)
30000
20000
10000
0
0
2
4
6
8
Time (hrs)
OG1RF
ΔdsbA

B.

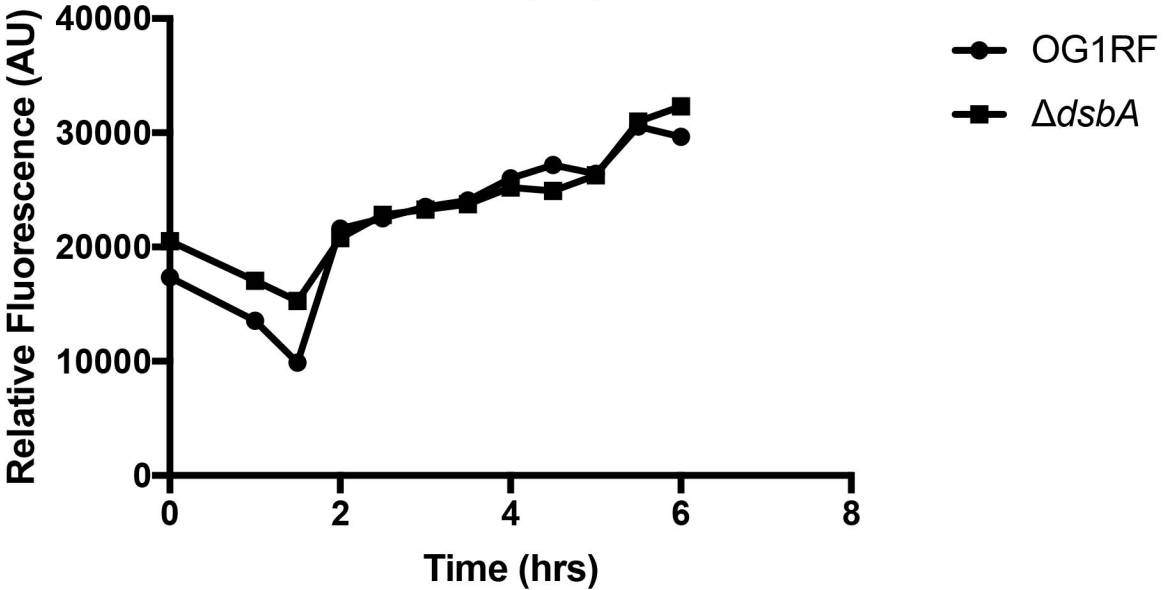
Relative Fluorescence (AU)
40000
30000
20000
10000
0
0
2
4
6
8
Time (hrs)
OG1RF
ΔdsbA

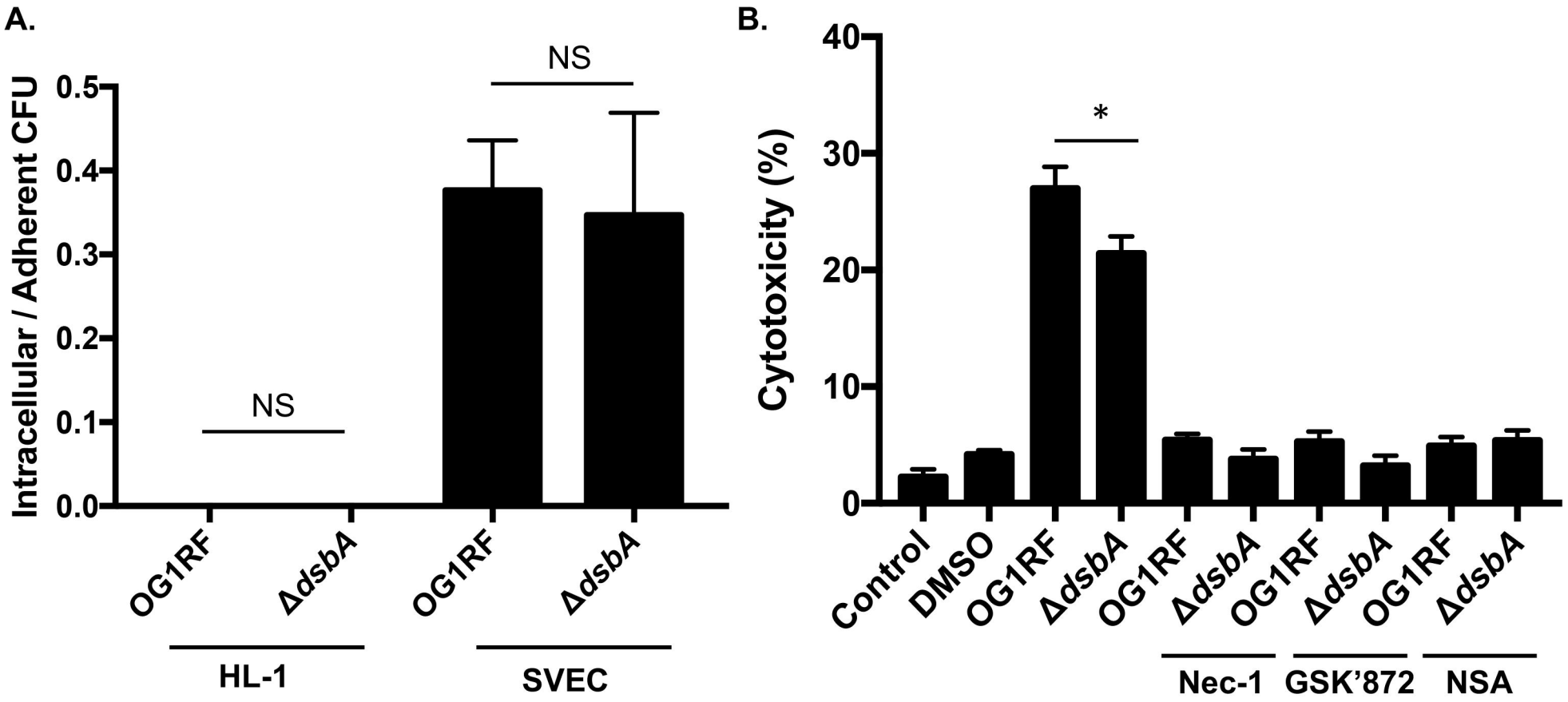
A.
Intracellular / Adherent CFU
0.5
0.4
0.3
0.2
0.1
0.0
NS
NS
OG1RF
ΔdsbA
OG1RF
ΔdsbA
HL-1
SVEC
B.
Cytotoxicity (%)
40
30
20
10
0
*
Control
DMSO
OG1RF
ΔdsbA
OG1RF
ΔdsbA
OG1RF
ΔdsbA
OG1RF
ΔdsbA
Nec-1
GSK'872
NSA